

# Radiative damping and emission signatures of strong superluminal waves in pulsar winds

Iwona Mochol and John G. Kirk

*Max-Planck-Institut für Kernphysik, Postfach 10 39 80, 69029 Heidelberg, Germany*

iwona.mochol@mpi-hd.mpg.de, john.kirk@mpi-hd.mpg.de

## ABSTRACT

We analyse the damping by radiation reaction and by Compton drag of strong, superluminal electromagnetic waves in the context of pulsar winds. The associated radiation signature is found by estimating the efficiency and the characteristic radiation frequencies. Applying these estimates to the gamma-ray binary containing PSR B1259–63, we show that the GeV flare observed by Fermi-LAT can be understood as inverse Compton emission by particles scattering photons from the companion star, if the pulsar wind termination shock acquires a precursor of superluminal waves roughly 30 days after periastron. This constrains the mass-loading factor of the wind  $\mu = L/\dot{N}mc^2$  (where  $L$  is the luminosity and  $\dot{N}$  the rate of loss of electrons and positrons) to be roughly  $6 \times 10^4$ .

*Subject headings:* plasmas – pulsars: general – pulsars: individual (PSR B1259-63) – radiation mechanisms: non-thermal – waves – stars: winds, outflows

## 1. Introduction

Pulsar winds contain electromagnetic fields, relativistic electrons, positrons and possibly ions, and are thought to power the diffuse, broad band continuum emission observed from pulsar wind nebulae. Their energetics is dominated by Poynting flux, but the nebulae outside their termination shocks appear to contain electromagnetic fields and relativistic leptons approximately in equipartition (for a recent review, see Kirk et al. 2009). The implied conversion process is still not completely understood, although it is becoming clear that only the wave-like, oscillating components of the fields must be dissipated at or inside the

termination shock, because the phase-averaged component can dissipate in the bulk of the nebula (Begelman 1998; Porth et al. 2013) without violating observational constraints.

Although dissipation of the wave component in a freely expanding wind is possible (Kirk & Skjæraasen 2003; Lyubarsky 2010) most current work concentrates on the structure of the shock itself, which is located close to the point where the ram pressure of the pulsar wind drops to that of the confining nebula. Two scenarios are under discussion: In the first, the wave is treated as a series of current sheets (the “striped wind”) which are compressed as they pass through an MHD shock, and subsequently dissipate by driven magnetic reconnection (Lyubarsky 2003; Pétri & Lyubarsky 2007; Lyubarsky & Liverts 2008; Sironi & Spitkovsky 2011, 2012). In the second, the wave converts into strong electromagnetic waves of superluminal phase velocity which dissipate in an extended shock precursor (Arka & Kirk 2012; Mochol & Kirk 2013; Amano & Kirk 2013).

These scenarios are, in a sense, complementary, since the former appears to operate at relatively high plasma density, whereas the latter requires the density to be below a certain threshold. However, observational constraints on the plasma density in pulsar winds are loose, and it is not clear which scenario operates in any given pulsar. The purpose of this paper is to show that it might be possible to distinguish between these scenarios observationally, because they can be expected to have distinct radiation signatures. The underlying physical reason is that the particles in an extended electromagnetic shock precursor radiate at relatively low energy, before thermalisation at a shock front, whereas, in the driven reconnection scenario, particles are expected to thermalise before they have a chance to radiate.

In Section 2 we summarise the properties of the electromagnetic waves relevant in a shock precursor. Section 3 then discusses damping by the classical radiation reaction force and by the Compton drag force exerted when electrons and positrons moving in the waves scatter ambient photons. These dissipation processes lead to synchrotron-like emission (called synchro-Compton emission) and inverse Compton emission, respectively. Estimates of the resulting radiation signature are applied in Section 4 to the wind from PSR B1259–63, which is in an eccentric orbit around a luminous Be star. This system is particularly interesting, since the termination shock has the potential to transit between the driven reconnection and the electromagnetic precursor scenarios as a function of orbital phase. We suggest that such a transition can produce a flare similar to the gamma-ray flare observed by Fermi-LAT (Abdo et al. 2011; Tam et al. 2011) a few days after periastron.

## 2. Electromagnetic precursors and radiation damping

### 2.1. The cut-off radius

Low amplitude electromagnetic waves can propagate in an electron-positron pair plasma if their frequency exceeds the local plasma frequency. This statement holds for circularly polarised waves of arbitrary amplitude, provided the plasma frequency is defined in terms of the local phase-averaged *proper* density  $n$  of the electron or positron fluid:  $\omega_p = (8\pi ne^2/m)^{1/2}$ . In a pulsar wind, waves are driven at the rotation frequency of the pulsar, and the radial decrease of proper density leads to the existence of a critical minimum radius for electromagnetic wave propagation.

The particle flux density at distance  $r$  from the pulsar and the energy (in units of  $mc^2$ ) carried per particle in the wind are:

$$J = \dot{N} / (r^2 \Omega_s) \quad (1)$$

and

$$\mu = L_{sd} / \dot{N} mc^2, \quad (2)$$

where  $\dot{N}$  is the  $e^\pm$  production rate of the pulsar,  $\Omega_s$  the solid angle occupied by the wind, and  $L_{sd}$  is the luminosity carried by the wind, which is usually assumed to equal the spin-down power. The parameter  $\mu$  corresponds to the maximum possible particle Lorentz factor  $\gamma$ , that is achieved only when the entire energy flux is carried by cold particles. From the definition of  $J$  and  $\mu$ , and the inequalities  $J < 2\gamma cn < 2\mu cn$ , one finds

$$r > \frac{a_L c}{\mu \omega_p} \quad (3)$$

where  $a_L$  is a — typically very large — dimensionless parameter related to the luminosity per unit solid angle:

$$\begin{aligned} a_L &= \sqrt{\frac{4\pi e^2 L_{sd}}{m^2 c^5 \Omega_s}} \\ &= 3.4 \times 10^{10} (L_{sd}/10^{38} \text{ erg s}^{-1})^{1/2} (\Omega_s/4\pi)^{-1/2} \end{aligned} \quad (4)$$

This suggests the use of a dimensionless radius coordinate:

$$R = r\omega\mu/ca_L \quad (5)$$

and a detailed treatment indeed reveals that the cut-off radius for both linear and circular polarised waves lies very close to, but slightly outside  $R = 1$  (Arka & Kirk 2012).

## 2.2. Subluminal modes

For  $R < 1$ , it is expected that the MHD approximation is adequate to describe the plasma dynamics. The oscillating components of the fields can be assumed to be carried along with the plasma in a quasi-stationary pattern containing a combination of current sheets and/or magnetic shear, all moving at subluminal phase speed. But this subluminal mode is not restricted to small radius; it exists out to arbitrary large distance. Its properties depend on  $\mu$  and on the magnetisation parameter  $\sigma_0$ , defined as the ratio of Poynting flux to kinetic energy flux. A pulsar wind is expected to be cold, supermagnetosonic and Poynting-flux dominated when launched, which implies  $\mu \gg 1$  and  $\sigma_0 \lesssim \mu^{2/3}$ . The radial momentum per particle,  $\nu mc$ , is in this case almost equal to the energy carried radially per particle, divided by  $c$ :

$$\nu \approx \mu - \frac{\sigma_0}{2\mu}. \quad (6)$$

Subluminal modes emit very little radiation, since the particle trajectories in them are almost ballistic. An observable signal can be expected only from inverse Compton scattering in the presence of a dense ambient photon field (Ball & Kirk 2000; Bogovalov & Aharonian 2000; Cerutti et al. 2008). The magnetisation stays close to its initial value up to very large distance  $R \sim \mu/\sigma_0$ , after which it gradually falls off, as the Poynting flux converts to particle energy. This phase may be relevant in a charge-starved blazar jet (Kirk & Mochol 2011) but it is not likely to be encountered in a pulsar wind, which is confined by either the interstellar medium or the wind of a companion star.

## 2.3. Jump conditions and superluminal modes

At sufficiently large radius, the MHD approximation, which excludes electromagnetic waves of superluminal phase speed, can fail. In particular, if the termination shock of a pulsar wind lies at  $R > 1$ , a precursor dominated by these waves can form. The dynamics of such a structure is complex, containing both forward and backward propagating waves (Amano & Kirk 2013), and it is not clear that a steady state is established. However, in order to gain insight into the possible configurations, and the radiation signature they might emit, it is useful to study a highly simplified case that is accessible analytically. In this paper, therefore, we concentrate on a solution in which the precursor is described by a steady, circularly polarised wave in a cold, two-fluid (electron and positron) model.

Initially, this wave must carry the same particle, energy and radial momentum fluxes as the incoming subluminal mode. This leads to a set of jump conditions that determine the

phase-averaged wave quantities at launch (Arka & Kirk 2012):

$$J = 2cnp_{\parallel} \quad (7)$$

$$\mu = \left( \gamma + \frac{\beta_w \gamma_w^2 p_{\perp}^2}{p_{\parallel}} \right) \quad (8)$$

$$\nu = \left( p_{\parallel} + \frac{(1 + \beta_w^2) \gamma_w^2 p_{\perp}^2}{2p_{\parallel}} \right) \quad (9)$$

where  $\gamma$ ,  $p_{\parallel}$  and  $p_{\perp}$  are the Lorentz factor, the parallel momentum and the magnitude of the transverse momenta of the fluids (the latter both in units of  $mc$ ). Together with the proper density  $n$ , these quantities are phase-independent. The wave group speed  $\beta_w (= ck/\omega)$  and corresponding Lorentz factor,  $\gamma_w$ , follow from the dispersion relation

$$\omega^2 = \omega_p^2 + c^2 k^2. \quad (10)$$

The amplitude  $E$  of the wave electric field, which is purely transverse, is related to the transverse momentum

$$E = mcp_{\perp}\omega/e \quad (11)$$

and can take on arbitrarily large values, as can also  $p_{\parallel}$ . Note, however, that for a given lab. density, these quantities enter into the definition of the plasma frequency, allowing large amplitude waves to propagate through dense plasmas.

For a given set of parameters  $\mu$  and  $\sigma_0$  (and, hence  $\nu$ ) of the incoming subluminal mode there are, at each radius outside the cut-off, two solutions to the jump conditions (7–9), corresponding to a free-escape and a confined mode. In a shock precursor, the latter is the relevant solution. Except very close to  $R = 1$ , it is characterised by a relatively large transverse momentum. This can be exploited to find an approximate solution. From the continuity equation (7), and the definitions (1), (2) and (4), it follows that:

$$p_{\parallel} = \gamma_w^2 \mu / R^2. \quad (12)$$

Substituting this expression into (8) and (9) and observing that, for  $p_{\parallel} \ll \gamma$ , the particle contribution to the momentum flux is negligibly small, one finds, provided the flow remains

relativistic ( $\gamma \gg 1$ ),

$$\gamma \approx p_{\perp} \tag{13}$$

$$\approx \frac{\mu(1 - \beta_w)^2}{1 + \beta_w^2} \tag{14}$$

$$p_{\parallel} \approx \frac{\mu(1 - \beta_w)^3}{2(1 + \beta_w)(1 + \beta_w^2)} \tag{15}$$

$$R \approx \frac{2^{1/2}(1 + \beta_w^2)^{1/2}}{(1 - \beta_w)^2}. \tag{16}$$

Thus, all quantities at the launching point are approximately determined by the single parameter  $R$ , or, alternatively,  $\beta_w$ .

### 3. Radiation damping

Since the precursor extends over a distance that is at most comparable to the radius of the termination shock, it can be regarded for the purposes of our estimates as a plane wave. The damping effect of radiation can then be treated using a perturbative approach, as originally presented for the linearly polarised case by Asseo et al. (1978). The procedure is closely related to that described for spherical wave propagation in the short wavelength approximation described in Mochol & Kirk (2013). In the ultra-relativistic limit, the radiation-reaction force is almost anti-parallel to the particle momentum, and has time-like and  $x$ -components (Landau & Lifshitz 1975)

$$g^{0,1} \approx -\frac{2e^4}{3m^3c^6} E^2 |\gamma - \beta_w p_{\parallel}|^2 (\gamma, p_{\parallel}) . \tag{17}$$

Equations (9) and (10) of Mochol & Kirk (2013), simplified to the case of circular polarisation (in which case the phase-averaging is trivial) and to planar geometry, acquire the terms  $ng^0$  and  $ng^1$  on their respective right-hand sides. The energy and entropy equations — (9) and (12) of that paper — then take the form

$$\frac{d}{dx} \left( 2np_{\parallel}\gamma + \frac{\beta_w E^2}{4\pi mc^2} \right) = ng^0 \tag{18}$$

$$\frac{d\gamma}{dx} = \frac{g^1 - \beta_w g^0}{2\Delta} \tag{19}$$

By introducing the space-dependent magnetisation parameter

$$\sigma = \frac{\beta_w p_{\perp}^2 R^2}{\mu\gamma} \tag{20}$$

and using the definitions

$$\delta = p_{\parallel} - \beta_w \gamma \quad (21)$$

$$\Delta = \gamma - \beta_w p_{\parallel} \quad (22)$$

$$\epsilon = \frac{2e^2 \omega}{3mc^3}. \quad (23)$$

these can be written as <sup>1</sup>

$$\frac{2\mu}{\epsilon a_L} \frac{d}{dX} [\gamma (1 + \sigma)] = -\frac{\gamma \Delta^2 p_{\perp}^2}{p_{\parallel}} \quad (24)$$

$$\frac{2\mu}{\epsilon a_L} \frac{d\gamma}{dX} = -\delta \Delta p_{\perp}^2 \quad (25)$$

where the cartesian coordinate along the propagation direction  $x$  has been normalised to the cut-off radius, in analogy with Eq. (5):  $X = x\omega\mu/(ca_L)$ .

Note that  $\sigma$ ,  $\delta$ ,  $\Delta$ ,  $\gamma$ ,  $p_{\parallel}$ ,  $p_{\perp}$  and  $\beta_w$  are all functions of  $X$ , although the argument has been omitted to simplify the notation. For superluminal waves,  $\Delta > 0$ , implying that the Poynting flux, which is proportional to  $\gamma\sigma$ , decreases monotonically with  $X$  for positive particle flux ( $p_{\parallel} > 0$ ):

$$\frac{2\mu}{\epsilon a_L} \frac{d}{dX} (\gamma\sigma) = -\frac{\Delta p_{\perp}^2 (1 + p_{\perp}^2)}{p_{\parallel}} \quad (26)$$

On the other hand, radiative reaction causes the particle Lorentz factor  $\gamma$  to increase when the wave moves faster than the particles, i.e., when  $p_{\parallel}/\gamma - \beta_w = \delta/\gamma < 0$ , but decrease when the particles are faster.

Equations (26) and (25) show that the ratio of the rate of change of Poynting flux to the rate of change of  $\gamma$  is  $(1 + p_{\perp}^2)/(p_{\parallel}\delta)$ , which is large except very close to the point  $R = 1$ . Thus, on launch, the wave starts to convert Poynting flux into radiation, whilst leaving the Lorentz factor of the charged fluids, and, therefore, the flux of kinetic energy unchanged. This reduction in Poynting flux is attributable entirely to a decrease of the wave group speed  $\beta_w$ , or, equivalently, an increase of the phase speed and of the wavelength of this mode. Ultimately, when the wavelength approaches the radial distance from the pulsar, the short wavelength (plane-wave) approximation used to derive the governing equations breaks down. At this point, however, the incoming Poynting flux has, to a good approximation, been completely converted into radiation. The (dimensionless) length-scale  $X_{\text{diss}}$  on which this happens follows from eq (26):

$$X_{\text{diss}} = \frac{2\mu}{\epsilon a_L} \left( \frac{\gamma\sigma p_{\parallel}}{\Delta p_{\perp}^2 (1 + p_{\perp}^2)} \right) \quad (27)$$

---

<sup>1</sup>We note that the entropy equation given by Asseo et al. (1978) (eq 32 in that paper) — contains an error arising from the neglect of first-order terms in Faraday’s equation (eq 14).

where the values of  $\gamma$ ,  $\sigma$ ,  $p_{\parallel}$ ,  $p_{\perp}$  and  $\Delta$  are those at launch, which follow from the jump conditions. When the dissipation length exceeds the radial distance to the pulsar, the plane-wave approximation breaks down well before the Poynting flux has been converted into radiation. To take account of this, we estimate the efficiency  $\eta$  of conversion of spin-down power into radiation in the precursor wave as follows:

$$\eta = \begin{cases} \sigma/(1 + \sigma) & \text{for } X_{\text{diss}} < R \\ \sigma R/[X_{\text{diss}}(1 + \sigma)] & \text{for } X_{\text{diss}} > R \end{cases} \quad (28)$$

In addition to damping by the radiation reaction term in the fluid equation of motion, damping of waves in a pulsar wind can also result from Compton drag — the force that results from the scattering of individual, ambient photons by the relativistically moving electrons and positrons that make up the two cold fluids. In general, this effect can be quite complicated, since it depends on both the angular and spectral distributions of the target photon field. Ambient photon fields such as the light from distant stars, the cosmic microwave background or synchrotron radiation from the pulsar wind nebula can be assumed to be isotropic, which considerably simplifies the computations. However, photons radiated by the neutron star surface or originating from a close binary companion are highly anisotropic, which has important consequences for radial winds (Kirk et al. 1999; Bogovalov & Aharonian 2000). Nevertheless, since our treatment is restricted to an electron velocity with a large angular spread,  $p_{\perp}/p_{\parallel} \gg 1$ , the average drag is approximately equal to that found assuming the target photons to be isotropic.

In pulsar winds, the target photons, whose characteristic frequency will be denoted by  $\nu_0 \equiv x_0 mc^2/h$ , can be assumed to be soft, and the drag force is approximately anti-parallel to the fluid velocity, as it is in the case of radiation reaction. For scatterings that take place in the Thomson regime,  $\gamma x_0 < 1$ , the computation is relatively simple. However, in the case of gamma-ray binaries, the drag exerted by photons from the companion star is reduced significantly by the Klein-Nishina effect. The resulting expression for the dissipation length  $X_{\text{diss}}$  including both the radiation reaction term and the Compton drag is

$$X_{\text{diss}} = \frac{2\mu}{\epsilon a_L} \left( \frac{\gamma \sigma p_{\parallel}}{\Delta p_{\perp}^2 (1 + p_{\perp}^2)} \right) \left( 1 + \frac{G(\gamma, x_0) \gamma_{\text{ic}}^2}{\Delta^2} \right)^{-1} \quad (29)$$

where  $G(\gamma, x_0)$  is the reduction factor due to Klein-Nishina effects ( $G(\gamma, x_0) \rightarrow 1$  for  $\gamma x_0 \rightarrow 0$  such that  $\gamma x_0^{1/3} \rightarrow \infty$ ) originally given by Jones (1965), see also Kirk et al. (1999, equation (A10)), and the energy density of target radiation  $U_{\text{rad}}$  enters via an effective Lorentz factor  $\gamma_{\text{ic}}$  at which the two terms have approximately equal magnitudes

$$\gamma_{\text{ic}} = \left( \frac{2\sigma_T U_{\text{rad}} c^2}{e^2 \omega^2} \right)^{1/2} \quad (30)$$



with  $\sigma_T$  the Thomson cross section.

Adopting the energy density of the cosmic microwave background,  $\gamma_{\text{ic}} = 7.3 \times P_{\text{sec}}$ , where  $P_{\text{sec}}$  is the pulsar period in seconds. Thus, provided the termination shock is located sufficiently close to the pulsar to produce relativistic particles in the precursor ( $R \ll \mu$ ), inverse Compton scattering with this radiation field as a target is energetically unimportant. In this case, the condition for a substantial fraction of the spin-down power to be converted into radiation,  $X_{\text{diss}} < R$ , reads:

$$\frac{1}{2} (\epsilon a_L \mu^2) f(R) > 1 \quad (31)$$

where

$$f(R) = \frac{\Delta (1 + p_{\perp}^2)}{\beta_w p_{\parallel} \mu^2 R} \quad (32)$$

The function  $f$  is plotted in Fig. 1. For relativistic flows, it is a function of  $R$  only, as indicated. Using the approximate jump conditions (13–14), according to which  $\gamma \rightarrow \mu/R$  and  $p_{\parallel} \rightarrow \mu/(2R)^{3/2}$  for large  $R$ , one finds

$$f(R) \approx 2\sqrt{2}R^{-5/2} \text{ for } R \gg 1 \quad (33)$$

which demonstrates that the importance of radiation losses falls off rapidly as the termination shock radius becomes large. However, close to the cut-off radius,  $f \sim 1$ , so that, assuming the termination shock lies close to this point, i.e. at

$$r \sim 10^{16} L_{38}^{1/2} P_{\text{sec}} \mu_4^{-1} \text{ cm} \quad (34)$$

(where  $\mu = \mu_4 \times 10^4$ ), the condition for the precursor to radiate a significant fraction of the wind luminosity as a result of damping by radiation reaction is roughly

$$\epsilon a_L \mu^2 = 1.3 \times 10^{-4} \mu_4^2 L_{38}^{1/2} P_{\text{sec}}^{-1} \quad (35)$$

$$> 1. \quad (36)$$

With Compton drag included in the definition of  $X_{\text{diss}}$ , the radiation efficiency (28) can be split into two terms. The first,  $\eta_{\text{sc}}$ , arises from radiation reaction and channels energy into synchrotron-like emission produced by the curvature in the fluid trajectories, a process that has been called “synchro-Compton” emission (Rees 1971). The second term,  $\eta_{\text{ic}}$ , arises from Compton drag and channels energy into inverse Compton scattered photons:

$$\eta_{\text{sc}} = \eta / \left( 1 + \frac{G(\gamma, x_0) \gamma_{\text{ic}}^2}{\Delta^2} \right) \quad (37)$$

$$\eta_{\text{ic}} = \eta / \left( 1 + \frac{\Delta^2}{G(\gamma, x_0) \gamma_{\text{ic}}^2} \right) \quad (38)$$

In the idealised, cold, two-fluid model used here, both radiation processes produce photons in narrow spectral bands. The synchro-Compton emission peaks at a (dimensionless) photon energy given by (e.g., Blandford 1972)

$$\bar{x}_{\text{sc}}(\gamma, p_{\perp}) = 0.4\gamma^2 p_{\perp} (\hbar\omega/mc^2), \quad (39)$$

whereas the peak energy of inverse Compton scattered photons can be estimated as

$$\bar{x}_{\text{ic}}(\gamma, x_0) = (4/3)\sigma_{\text{T}}x_0\gamma^2 G(\gamma, x_0)/\langle\dot{N}_{\gamma}\rangle, \quad (40)$$

where  $\dot{N}_{\gamma}$  is the scattering rate divided by the density of target photons and  $\langle\dots\rangle$  indicates an angle average, i.e.,

$$\langle\dot{N}_{\gamma}\rangle = \frac{c}{2\gamma x_0} \int_{\gamma x_0(1-\beta)}^{\gamma x_0(1+\beta)} dx' x' \sigma_{\text{KN}}(x') \quad (41)$$

where  $\beta = \sqrt{\gamma^2 - 1}/\gamma$ , and  $\sigma_{\text{KN}}(x)$  is the total Klein-Nishina cross section for a photon of energy  $xmc^2$  (see Jones 1965; Kirk et al. 1999).

#### 4. Application to PSR B1259–63/SS2883

The radiation efficiencies, determined by Eqs (28), (29), (37) and (38), together with the peak photon energies (39) and (40) may be used to estimate the radiation signature of a potential electromagnetic precursor to the pulsar wind termination shock, given the pulsar’s angular frequency  $\omega$ , the parameter  $a_{\text{L}}$ , defined in eq (4), the distance  $r_{\text{ts}}$  of the shock from the pulsar, the energy density and characteristic frequency of the dominant soft photon targets and the mass-loading parameter  $\mu$ .

In this section we use pulsar PSR B1259–63 as an illustrative example. This intensively observed and modelled object is a member of the gamma-ray binary class (Dubus 2006), and was the first source to be discovered in TeV gamma-rays by the HESS collaboration (Aharonian et al. 2005). Its angular frequency is  $131\text{ s}^{-1}$  and its spin-down luminosity is  $8.3 \times 10^{35}\text{ erg s}^{-1}$ , giving  $a_{\text{L}} = 3 \times 10^9$ , assuming the pulsar wind occupies a solid angle of  $4\pi\text{ sr}$ . The 3.4 yr orbit is eccentric, the separation between the two stars varying by roughly a factor of 14 between apastron and periastron, where it is approximately  $10^{13}\text{ cm}$ . Thus, the distance from the pulsar to that part of the termination shock that lies between the two stars is fairly tightly constrained. The dominant photon field that serves as a target for inverse-Compton scattering is provided by the luminous Be star SS2883. This leads to  $x_0 \approx 10^{-5}$  and

$$\gamma_{\text{ic}} = 1.4 \times 10^6 \left( \frac{L_{*}}{2.3 \times 10^{38}\text{ erg s}} \right)^{1/2} \left( \frac{d}{10^{13}\text{ cm}} \right)^{-1} \quad (42)$$

where  $d$  is the distance to the star and  $L_*$  its luminosity, and we have adopted as fiducial parameters those given by Negueruela et al. (2011), which indicate a somewhat more luminous and distant star than previously thought (e.g., Johnston et al. 1994).

The most difficult parameter to constrain observationally is the mass-loading  $\mu$ . It is related to the “multiplicity”  $\kappa$  associated with the pair creation mechanism close to the pulsar by  $\mu = a_L/4\kappa$ , but this parameter is also difficult to estimate. Modelling of the nonthermal emission near periastron suggests  $\mu \approx 10^6$  (Kirk et al. 1999; Kong et al. 2012), and identifying the spectral break in keV range with the low energy cut-off of the synchrotron emission associated with the relativistic wind suggests a similar value  $\mu \approx 4 \times 10^5$  (Uchiyama et al. 2009). These rough estimates should be considered as upper limits, since they do not take into account the possibility that some particles in the wind might not be accelerated to high energy at the shock. Taking them at face value, places the distance from the pulsar of the cut-off point for electromagnetic waves ( $R = 1$ ) at  $2.3 \times 10^{12}$  cm and  $6 \times 10^{12}$  cm, respectively, close to the stand-off distance of the shock from the pulsar at periastron. A low energy particle component would imply a larger cut-off radius, so that, close to periastron, the pulsar wind termination shock might not have an electromagnetic precursor, but could form one when, as the stars move apart, the confining pressure of the companion’s wind drops, and the shock emerges through the cut-off radius. If this happens, one should expect a new emission component to emerge, with the properties described in the previous section.

Around periastron passage of 2010, the system was detected by Fermi-LAT (Abdo et al. 2011; Tam et al. 2011). The most interesting aspect of these observations is a flare of 1 GeV photons detected about 30 days after the periastron passage. This emission forms a new, spectrally distinct component that carries a substantial fraction of the pulsar’s spin-down luminosity. It presents a challenge to models based on electrons accelerated at the termination shock (Kong et al. 2012), which assume strong Doppler-beaming, as well as to those based on electrons in the unshocked wind (Pétri & Dubus 2011; Khangulyan et al. 2011, 2012), which require an additional source of target photons. In an electromagnetic precursor, on the other hand, emission is beamed into the plane transverse to the flow and covers a large fraction of the sky. Also, the relatively low energy ( $\gamma \sim 10^4$ ) electrons and positrons remain in the emission region for a time that is a factor  $\gamma/p_{\parallel} \approx (8R)^{1/2}$  longer than that of radially propagating particles, thus enhancing the radiated power.

In Fig. 2 we plot the efficiencies  $\eta_{sc}$  and  $\eta_{ic}$  together with the peak photon energies  $\bar{x}_{sc}$  and  $\bar{x}_{ic}$  as functions of time after periastron, assuming the shock to be located mid-way between the two stars. The rapid switch-on apparent in this figure is somewhat arbitrary, since (i) we assume the precursor is created instantaneously with a linear extent comparable to the shock radius and (ii) the exact jump conditions were used in the calculation, for which

an estimate of the wind magnetisation parameter is needed — we adopt  $\sigma_0 = 100$ . However, these uncertainties apply only during the rising phase of emission, when the shock is close to the cut-off radius. After the peak of emission at day 30, when the dissipation length exceeds the precursor size, the approximate jump conditions, which do not depend on  $\sigma_0$  are an accurate approximation. Thus, the only unconstrained parameter,  $\mu$ , is fixed by the epoch of maximum radiative efficiency. To match this to the peak of the flare detected by Fermi-LAT, we choose  $\mu = 6 \times 10^4$ .

Between 30 and 100 days after periastron, Fig. 2 predicts a peak energy for the inverse-Compton photons that drops from a few GeV to about 1 GeV, and a corresponding power that drops from roughly 20% to 10% of the spin-down luminosity. The synchro-Compton emission lies in the optical band, but accounts for only a small fraction of the spin-down luminosity, and would be swamped by photons from the companion star. Given the highly simplified treatment used to make these estimates, such as the assumption of a spherically symmetric wind and of uniform conditions with vanishing phase-averaged fields over the entire shock front, these properties are in encouraging agreement with those of the observed flare.

If the electromagnetic precursor is responsible for the Fermi-LAT flare, then the emission should be present at all binary phases during which the termination shock lies outside the cut-off radius. Over most of the binary orbit, the efficiency would be too low to permit detection. In Fig. 2 it is assumed that the shock lies mid-way between the two stars. If this holds over the entire orbit, and if the mass-loading parameter remains constant, then an additional flare should occur between 100 and 30 days *before* periastron passage. This is ruled out by Fermi observations. However, the location of the shock front depends on the relative strengths of the pulsar and the companion star winds, which can be expected to differ in the pre- and post-periastron parts of the orbit, since the wind of the companion star is known to be highly anisotropic. Consequently, although a pre-periastron flare is predicted, and should be described by the same formalism, it is not necessarily expected to be symmetrically timed with respect to periastron, and, therefore, not necessarily peaked in the GeV band.

## 5. Conclusions

Radiation reaction and Compton drag can be important damping mechanisms of superluminal waves in the winds of short period pulsars, if they exist close to the cut-off radius. This damping extracts the Poynting flux from the wind directly by reducing the group velocity of the wave, using the particles at catalysts, i.e., without depleting the kinetic energy

flux. We have derived explicit expressions for the efficiency of extraction and for the spectral bands into which the energy is channelled, as functions of the pulsar wind parameters and the properties of the ambient photon field.

In the case of the gamma-ray binary containing the pulsar PSR B1259–63, all of these parameters except the mass-loading  $\mu$  are well-constrained. Assuming the waves are generated as precursors to the termination shock of this pulsar when it encounters the wind of the companion star, the mass-loading parameter determines the epoch of maximum extraction efficiency. Choosing  $\mu = 6 \times 10^4$  fixes this to coincide with the enigmatic gamma-ray flare detected from this object by Fermi-LAT. In this case, the overall efficiency and the peak frequency of the inverse Compton emission are in rough agreement with those observed, suggesting that the flare is caused by the emergence of the shock from the cut-off radius, accompanied by the creation of a precursor containing superluminal waves. This interpretation predicts another flare when the precursor disappears, but its timing depends on unknown properties of the wind of the companion star.

## REFERENCES

- Abdo, A. A. et al. 2011, *ApJ*, 736, L11, 1103.4108
- Aharonian, F. et al. 2005, *A&A*, 442, 1, arXiv:astro-ph/0506280
- Amano, T., & Kirk, J. G. 2013, *ApJ*, 770, 18, 1303.2702
- Arka, I., & Kirk, J. G. 2012, *ApJ*, 745, 108, 1109.2756
- Asseo, E., Kennel, C. F., & Pellat, R. 1978, *A&A*, 65, 401
- Ball, L., & Kirk, J. G. 2000, *Astroparticle Physics*, 12, 335, arXiv:astro-ph/9908201
- Begelman, M. C. 1998, *ApJ*, 493, 291, arXiv:astro-ph/9708142
- Blandford, R. D. 1972, *A&A*, 20, 135
- Bogovalov, S. V., & Aharonian, F. A. 2000, *MNRAS*, 313, 504, arXiv:astro-ph/0003157
- Cerutti, B., Dubus, G., & Henri, G. 2008, *A&A*, 488, 37, 0807.1226
- Dubus, G. 2006, *A&A*, 456, 801, arXiv:astro-ph/0605287
- Johnston, S., Manchester, R. N., Lyne, A. G., Nicastro, L., & Spyromilio, J. 1994, *MNRAS*, 268, 430

- Jones, F. C. 1965, *Physical Review*, 137, 1306
- Khangulyan, D., Aharonian, F. A., Bogovalov, S. V., & Ribó, M. 2011, *ApJ*, 742, 98, 1104.0211
- . 2012, *ApJ*, 752, L17, 1107.4833
- Kirk, J. G., Ball, L., & Skjaeraasen, O. 1999, *Astroparticle Physics*, 10, 31, arXiv:astro-ph/9808112
- Kirk, J. G., Lyubarsky, Y., & Petri, J. 2009, in *Astrophysics and Space Science Library*, Vol. 357, *Neutron Stars and Pulsars*, ed. W. Becker (Springer Berlin Heidelberg), 421, arXiv:astro-ph/0703116
- Kirk, J. G., & Mochol, I. 2011, *ApJ*, 736, 165
- Kirk, J. G., & Skjæraasen, O. 2003, *ApJ*, 591, 366, arXiv:astro-ph/0303194
- Kong, S. W., Cheng, K. S., & Huang, Y. F. 2012, *ApJ*, 753, 127, 1205.2147
- Landau, L. D., & Lifshitz, E. M. 1975, *The classical theory of fields*
- Lyubarsky, Y. 2010, *ApJ*, 725, L234, 1012.1411
- Lyubarsky, Y., & Liverts, M. 2008, *ApJ*, 682, 1436, 0805.0085
- Lyubarsky, Y. E. 2003, *MNRAS*, 345, 153, arXiv:astro-ph/0306435
- Mochol, I., & Kirk, J. G. 2013, *ApJ*, 771, 53, 1303.6434
- Negueruela, I., Ribó, M., Herrero, A., Lorenzo, J., Khangulyan, D., & Aharonian, F. A. 2011, *ApJ*, 732, L11, 1103.4636
- Pétri, J., & Dubus, G. 2011, *MNRAS*, 417, 532, 1104.4219
- Pétri, J., & Lyubarsky, Y. 2007, *A&A*, 473, 683
- Porth, O., Komissarov, S. S., & Keppens, R. 2013, *MNRAS*, 431, L48, 1212.1382
- Rees, M. J. 1971, in *IAU Symposium*, Vol. 46, *The Crab Nebula*, ed. R. D. Davies & F. Graham-Smith, 407
- Sironi, L., & Spitkovsky, A. 2011, *ApJ*, 741, 39, 1107.0977
- . 2012, *Computational Science and Discovery*, 5, 014014, 1208.4998

Tam, P. H. T., Huang, R. H. H., Takata, J., Hui, C. Y., Kong, A. K. H., & Cheng, K. S. 2011, *ApJ*, 736, L10, 1103.3129

Uchiyama, Y., Tanaka, T., Takahashi, T., Mori, K., & Nakazawa, K. 2009, *ApJ*, 698, 911, 0904.1238

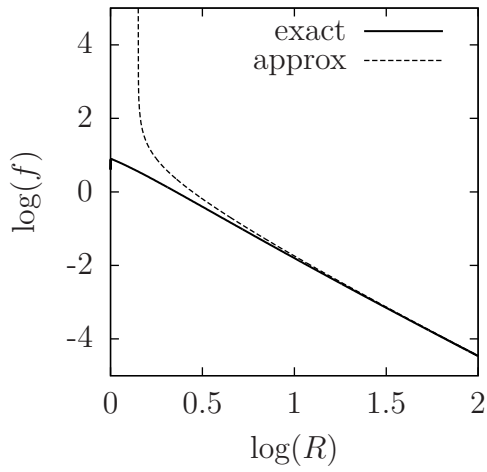


Fig. 1.— The function  $f(R)$  defined in Eq. (32) that determines the efficiency of synchro-Compton radiation, as a function of the dimensionless radius  $R$ . The curves labelled “exact” and “approx” are calculated using the exact and approximate jump conditions, defined by Eqs (7–9) and Eqs (13–16) respectively.



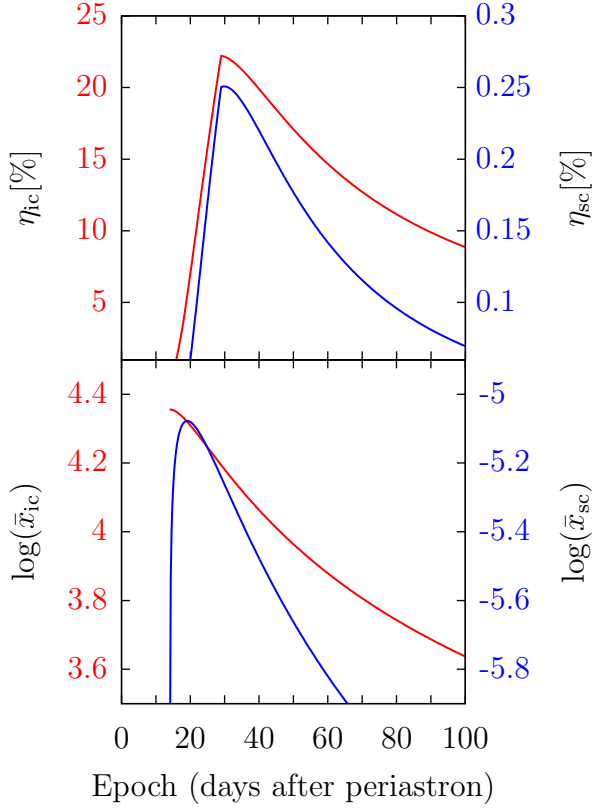


Fig. 2.— The efficiencies and peak energy bands of synchro-Compton (blue curves) and inverse Compton emission (red curves) from an electromagnetic shock precursor, calculated for  $\mu = 6 \times 10^4$  and  $\sigma = 100$ , as a function of the time (in days) after periastron for the binary system containing PSR B1259–63. The stellar and orbital parameters are taken from Negueruela et al. (2011) and the shock is assumed to be located mid-way between the two stars.